Cohesion induced deepening transition of avalanches

Chun-Chung Chen
Department of Physics, University of Washington, Seattle, Washington 98195
(Dated: February 1, 2008)

A directed avalanche model with a control parameter is introduced to describe the transition between cohesive and noncohesive granular material. The underlying dynamics of the process can be mapped to interface growth model. In that representation, a continuous phase transition separates the rough phase and the flat phase. In the avalanche formulation, this corresponds to a transition from deep to shallow avalanches. The scaling exponents of the avalanches indeed follow those of the underlying interface growth in both phases and at the transition point. However, the mass hyperscaling relation is broken at the transition point due to the fractal nature of the avalanche and a hierarchy of critical directed percolation processes.

PACS numbers: 45.70.Ht, 05.65.+b, 05.70.Np, 47.54.+r

I. INTRODUCTION

Granular avalanches have received much attention since sandpile models are used as paradigms of so-called self-organized criticality [1]. However, observations of critical-type distributions of avalanches in real physical systems are still rare, with as a notable exception the recent rice pile experiments by Frette *et al.* [2]. It was suggested by Christensen *et al.* [3] that the anisotropy in the rice grains allows more stable packing configurations in a granular pile, and that this could be responsible for the successful observation of criticality. Some of the recent attention has been drawn to avalanches in cohesive granular materials with the premise that cohesion will also allow the sand more packing configurations and thus increase the likelihood of observing critical scaling behavior. While the goal of finding criticality in cohesive sandpiles remains to be fulfilled even after the experimental work by Quintanilla *et al.* [4], the effect of cohesion in granular avalanches represents an interesting direction for a theoretical study.

In this article, we'll use the discrete-height version of the sandbox (DHSB) model introduced in Ref. [5] for an unloading sandbox (Fig. 1) to understand the effects of cohesion in directed avalanche systems. In the following section, we'll discuss how we can model cohesiveness in avalanche systems. In Sec. III, we'll review the DHSB model and introduce a cohesion parameter. Previous results in Refs. [5, 6] represent a special case of the model where the system is in the deep avalanche phase with the cohesion parameter $p = 1/2$. In Sec. IV, we describe the step-flow random-deposition (SFRD) interface growth model which underlies the DHSB model and the directed percolation (DP) roughening transition of the SFRD model. In Sec. V, we focus on the two deterministic limits of the model and present the exact solution in one of these limits. In Sec. VI, numerical results for the avalanches in the flat phase of the interface model are presented. In Sec. VII, we investigate the scaling behavior at the transition point where the interface roughness increases logarithmically in time. We show that the avalanche-scarred sand surface, while being rougher than nonscarred ones, retains the same scaling exponent of the roughness in the thermodynamic limit. However, we'll also show that at the transition point, the violation of mass hyperscaling relation spoils the reduction to two independent exponents established in Ref. [6]. We'll summarize our results in Sec. VIII.

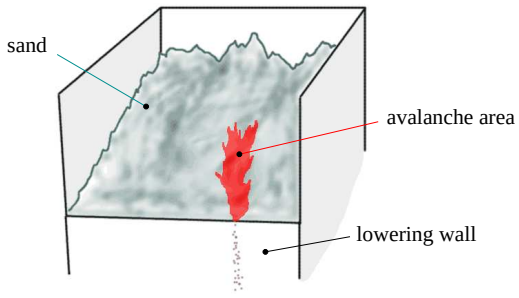

FIG. 1: A sandbox system. The rectangular box is filled with sand. One of the retaining wall can be lowered slowly to let out the sand in a sporadic way forming distinct avalanche events.

II. TUNABLE PARAMETER FOR COHESION

One interesting characters of cohesion in sand is that it possesses hysteresis behavior. Consider building a sand castle on a beach. It's common sense that we'll need to add water to the sand before we can shape it into a standing castle. However, without disturbance, the sand castle can somehow maintain its shape even after it dries out [7]. The moisture in sand increases the cohesion between the sand particles [8] and allows one to manipulate the sand into a stable shape that, while not as attainable, is more or less an equally valid stable shape for dry sand.

In accounting for this standing-sand-castle effect, we'll use the same stability condition for all cohesiveness of the sandbox. While, in reality, the space of possible stable configurations for wet and dry sand should not be exactly identical, in this article, we shall ignore this distinction

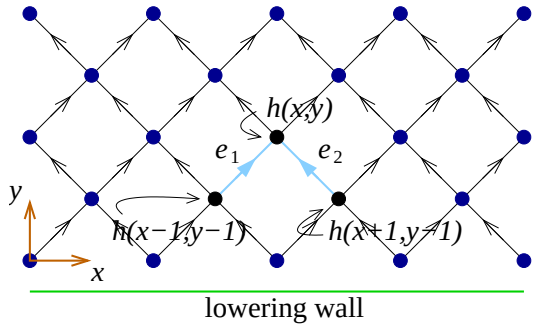

FIG. 2: The lattice structure of the two-dimensional discrete-height sandbox model. It corresponds to a top view of the sandbox with the lowering wall located at the bottom.

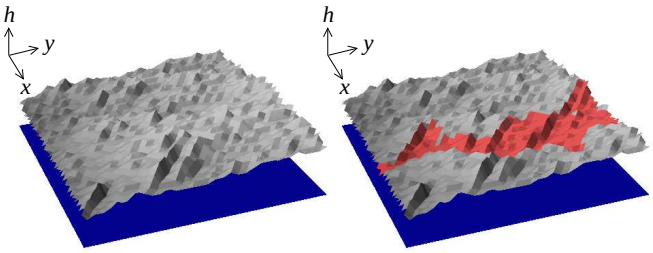

FIG. 3: A typical configuration of the discrete-height sandbox model before (left) and after (right) a system spanning avalanche. Sites participated in the avalanche are shaded darker. The system size $L_x \times L_y$ is 32×64.

to avoid complicating the rules too much.

On the other hand, the way an unstable sand surface topples surely depends on the cohesiveness. In the DHSB model discussed below, there are only two possible final stable states for any toppling site. We'll call them the minimal stable state and the maximal stable state. These two states are similar to the angle of repose and maximal stable angle in a real sandpile. However, in sandbox model, these states are microscopic while the "angles" of a real sandpile are macroscopic. We'll use a parameter p, which is a real number between 0 and 1, to represent the strength of cohesion. In the model, p is the probability for a toppling site of the sandpile to settle into the maximal stable state instead of the minimal one. For wet sand, the p is large, and for dry sand, the p is small.

III. DISCRETE-HEIGHT SANDBOX MODEL

With the discussion of the previous section in mind, let's review the dynamic rules of the discrete-height sandbox model. The surface of a sandbox (see Fig. 1) is represented by an integer height variable h defined on a two-dimensional square lattice which is tilted at 45° with respect to the lowering wall as illustrated in Fig. 2. This is equivalent to considering only the lattice points whose integer x and y coordinates satisfy the condition that $x + y$ is an even number. The lowering wall that drives the system by creating unstable sites is located at the $y = 0$ row and the activities in the system propagate only in the positive y direction. In our numerical simulations, the system is periodic in the x direction, which is parallel to the driving wall. The sizes of the system in the x and y directions are denoted by the numbers of sites L_x in each row and the number of rows L_y respectively.

As in most sandpile processes, the dynamics of the sandbox model is defined by a stability condition, a toppling rule, and a driving method. They are as follows. The stability condition of the DHSB is given by

$$h(x,y) \le \min\left[h(x-1,y-1), h(x+1,y-1)\right] + s_c \quad (1)$$

with $s_c = 1$, which represents the local maximal stable slope. The unstable sites in the system topple with the rule

$$h(x,y) \to \min\left[h(x-1,y-1), h(x+1,y-1)\right] + \eta, \quad (2)$$

where $\eta = 0$ with probability $1 - p$ and $\eta = 1$ with probability p. (In the earlier studies [5, 6], the value of p is always 1/2 .) This is the only place in the dynamics of the DHSB that the cohesion parameter p comes into play. The lowing wall which drives the system is implemented in the model by randomly picking one of the highest sites $(x_i, 0)$ on the $y = 0$ row and by reducing its height by 1:

$$h(x_i, 0) \to h(x_i, 0) - 1, \quad (3)$$

where i is the Monte Carlo time, which also serves as an age index for the avalanches.

A typical configuration of the DHSB before and after an avalanche is shown in Fig. 3. Since the toppling of a site on a given row y only affects the stability of the two sites immediately above it at the $y + 1$ row, we choose to update the system in a row-by-row fashion. For each avalanche, the entire system is stabilized by such a single sweep of topplings from $y = 0$ to $y = L_y$.

IV. UNDERLYING INTERFACE DYNAMICS

The underlying interface dynamics of the sandbox models is given by the step-flow random-deposition (SFRD) models with a two-step growth rule [5, 6] as illustrated in Fig. 4. The mapping between the sandbox system and the interface growth model involves identifying the y coordinate of the sandbox model with the time t of the interface growth. Each stable sandbox surface thus can be viewed as a space-time world-sheet configuration of the interface growth. Models similar to this generally belong to the Kardar-Parisi-Zhang (KPZ) universality class [9] with the critical exponents $\alpha = 1/2$, $\beta = 1/3$, and $z = \alpha/\beta = 3/2$ which characterize the scaling of interface roughness

$$W^2 \equiv \overline{(h - \bar{h})^2}. \quad (4)$$

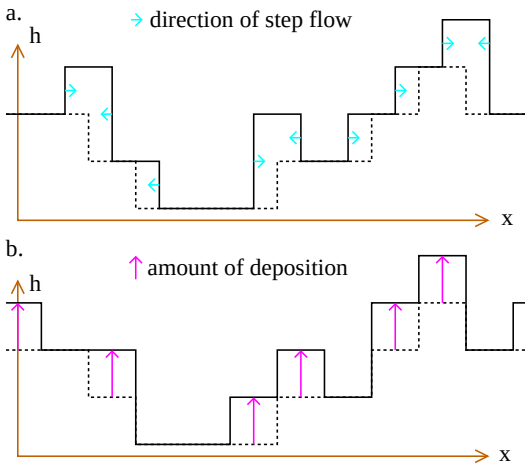

FIG. 4: Two-step growth of the discrete-height step-flow random-deposition interface growth model; (a) Steps flow by one unit to the right (left) when its size Δh is negative (positive); (b) Each site increases by one unit with a probability p.

Starting from a flat interface at $t = 0$, the interface grows rougher with

$$W \sim t^{\beta}. \tag{5}$$

And, after a characteristic time $t_c \approx L^z$, the roughness will saturate with a value

$$W \sim L^{\alpha} \tag{6}$$

depending on the system size L.

From the mapping introduced in Ref. [5], the avalanche exponents are given by

$$\tau_l = \frac{\sigma - 1 - \alpha}{z} = 2, \tag{7}$$

$$\tau_w = \sigma - z - \alpha = \frac{5}{2}, \tag{8}$$

and

$$\tau_\delta = \frac{\sigma - 1 - z}{\alpha} = 4 \tag{9}$$

for the distribution functions, $P_l(l) \sim l^{\tau_l}$, $P_w(w) \sim w^{\tau_w}$, and $P_\delta(\delta) \sim \delta^{\tau_\delta}$, of avalanche length l, width w, and depth δ. As defined in Ref. [5], the avalanche length l (width w) represents maximum y (x) distance of the toppling sites from the triggering point while the avalanche depth δ is the maximum height change of the toppling sites. The σ in these expressions was eliminated with the mass hyperscaling relation

$$\sigma = 2 + z + 2\alpha. \tag{10}$$

obtained from the compactness of the avalanche clusters, i.e., assuming $m \sim lw\delta$.

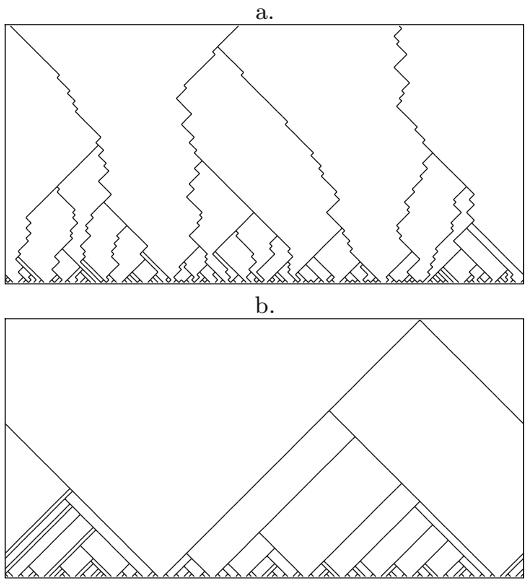

FIG. 5: Scar (edge lines of avalanche clusters) configurations of DHSB avalanches at the two deterministic limits; (a) $p = 0$; (b) $p = 1$.

However, the discrete-height version of the SFRD model undergoes a DP roughening transition at $p = p_c \approx 0.294515$ similar to those studied by Kertész and Wolf [10] also Alon *et al.* [11]. The KPZ scaling behavior only applies when the value of the control parameter p is greater than the critical value p_c. Below this transition point the interface is in a trivial flat state, where, for a stationary interface (interface time $y \to \infty$), the density of sites at the bottom $h = h_0$ layer is finite. The interface is thus *pinned* at this level and its growth rate becomes zero.

At the transition point $p = p_c$, we find the roughness of the SFRD interface diverges only logarithmically in time

$$W^2 \sim (\ln t)^{\gamma}, \tag{11}$$

with the exponent $\gamma \approx 1$ similar to that of the Kertész and Wolf's model as well as the restricted version of the models by Alon *et al.*.

V. DETERMINISTIC LIMITS

In the two limits, $p = 1$ and $p = 0$, the toppling process of the avalanches becomes deterministic and the sand surface topples down layer by layer. The only randomness in the process comes from the driving method (3), i.e., that we randomly lower one of the highest sites at the $y = 0$ row to trigger an avalanche. The typical avalanche scar configurations at these two limits are shown in Fig. 5. These are the edges of avalanche clusters left on the surface, some of which are partially erased by newer avalanches.

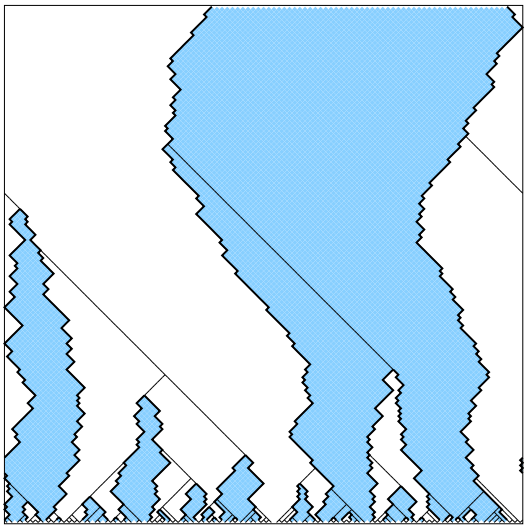

FIG. 6: The domains of odd (shaded region) and even (light region) sites on a DHSB surface at $p = 0$, separating them are domain walls that no avalanche will penetrate at this deterministic limit.

A. Domain walls at $p = 0$

The $p = 0$ limit runs into the complication that in the bulk of the system ($y > 0$) the sand surface goes down by 2 units at a time. Since $\Delta h \equiv h(x, y) - \min[h(x-1, y-1), h(x+1, y-1)] = 1$ is stable according to the stability condition (1), and the sites on the $y = 0$ row always goes down by 1 unit each time according to the driving method (3), the sites on the $y = 1$ row will only topple when their heights are 2 units higher than the triggering sites and they alway go down by 2 units to the same height of the triggering site according to the toppling rule (2). All the sites at higher rows will be locked into the same even-oddness as the sites triggering their toppling. Therefore, after all sites have participated in at least one avalanche, their even-oddness will be fixed for all subsequent topplings. This means the even-oddness of a site is preserved by the toppling process, and that the lines separating the even and odd sites thus form impenetrable domain walls for the avalanches (see Fig. 6). This hinders the applicability of the same type of analysis as presented below for the $p = 1$ limit. However, the numerical results in Sec. VI will show that the same scaling exponents as those of $p = 1$ case control this limit, too.

B. Exact solution at $p = 1$

The $p = 1$ limit has a nice solution. Since the sites in the bulk topple from $\Delta h = 2$ to $\Delta h = 1$, the sand surface indeed goes down only one layer at a time without the complications as the $p = 0$ case. An exact solution can be obtained by considering the avalanches taking place in such one single layer. For a brand-new layer, the two boundaries of the first avalanche open up linearly until the avalanche spans the system in the x direction and leaves two scar lines on the surface. The two boundaries of the second avalanche expand until they meet the scar lines created by the first avalanche. Then, they turn and follow those scar lines until they meet with each other and terminate the avalanche. Subsequent avalanches follow the same scenario. The maximum distance an avalanche cluster can expand from its triggering point to each side in the x direction is exactly half the distance from the nearest triggering point of the previous avalanches in the same layer on that side. As the triggering points are chosen in an uncorrelated manner, the maximum width w of an avalanche should follow the Poisson distribution

$$P_w(w) = \frac{\mu^w e^{-\mu}}{w!} \tag{12}$$

if μ is the average distance between the triggering points of the previous avalanches in the same layer in the stationary state. The avalanche under consideration could be any one of the avalanches happening in the same layer. Thus, we need to average over the number of avalanches n taking place before this one in the same layer. For a system of transverse size L_x, $n = L_x/\mu$, the integral can be carried out explicitly and gives

$$\int_0^\infty \frac{\mu^w e^{-\mu}}{w!} d\frac{1}{\mu} = \frac{(w-2)!}{w!} \sim w^{-2}, \tag{13}$$

which results in

$$\tau_l = \tau_w = 2. \tag{14}$$

The same results can also be derived from Eq. (7) and (8) by assuming $z = 1$ and $\alpha = 0$. Since the avalanches are compact, the hyperscaling relation (10) and other exponent relations (7)–(9) from Ref. [5] hold.

VI. SHALLOW-AVALANCHE PHASE

Below the transition point, the underlying interface model is in a flat phase where the bottom layer percolates with finite density. All the information of the initial configuration of the interface (the $y = 0$ row next to the wall) is wiped out at a time scale proportional to the sizes of the islands higher than the bottom layer in the initial state. (Without deposition, the sizes of these islands decrease linearly in time.) While the underlying interface model is in a trivial phase, much like the uncorrelated stationary state in Dhar and Ramaswamy's directed sandpile model [12], the avalanche distributions of the system may still exhibit power-law scaling. The numerical values of the scaling exponents shown in Fig. 7 confirm the power-law scaling of the distributions and they are similar to those values found at the $p = 1$ fixed point following $z = 1$ and $\alpha = 0$. While an exact solution is not available in this phase, we can understand

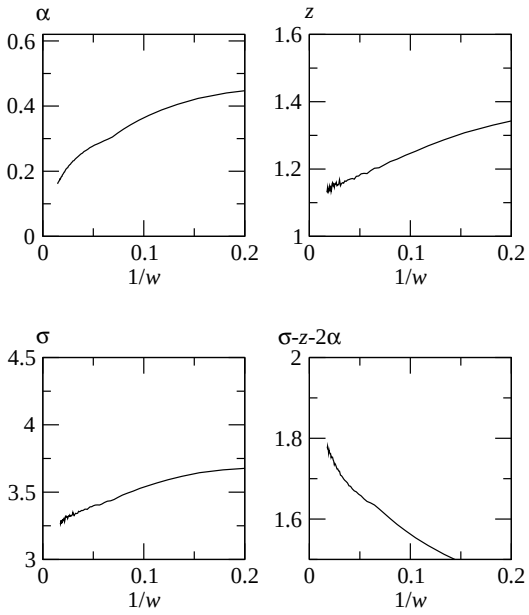

FIG. 7: Finite-size scaling (FSS) estimates of the scaling exponents versus inverse width $(1/w)$ of avalanche clusters for the DHSB avalanches in the shallow-avalanche phase (measured at $p = 0.1$). They are consistent with $\alpha = 0$ and $z = 1$.

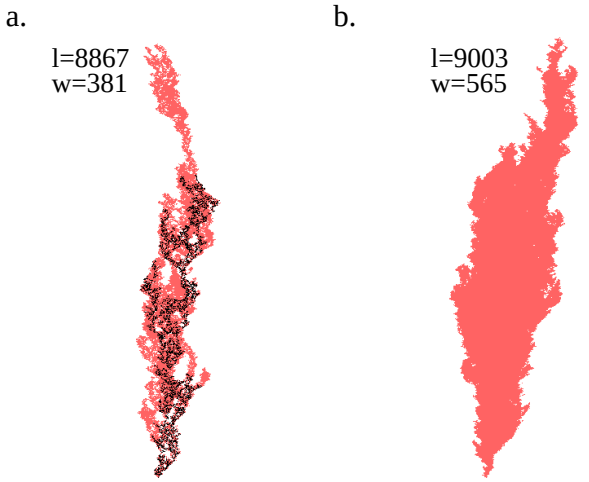

FIG. 8: Typical large avalanche cluster for DHSB (a) at the DP transition point; (b) in the deep avalanche phase ($p = 0.5$), triggered at lowering wall boundary at the bottom. The length l and width w of each avalanche are as labelled. Black area in the cluster of (a) is of sites that topple to the lowest height h_0 of the bottom layer. It shows the percolation of the bottom layer. One sees that the avalanche maintains a compact structure in the deep avalanche phase while becomes more fractal-like at the transition point.

the scaling exponent $z = 1$ from the perspective that the DP clusters triggered from single seeds in the percolating phase open up linearly $l \sim w$; and also that roughness exponent $\alpha = 0$ comes from that the interface is flat. However, a difference is that while $p < p_c$ represents an entire phase of shallow avalanches which should be controlled by an attractive fixed point, the $p = 1$ fixed point is unstable in the sense that the scaling behavior falls back to the KPZ universality class for any small deficiency in the cohesiveness p from the value 1.

VII. DP ROUGHENING TRANSITION

At the transition point $p = p_c$, the interface roughness diverges logarithmically thus the β and α exponents, defined by Eqs. (5) and (6), are both zero. Nonetheless, the dynamic exponent z has a nontrivial value $z_{\rm DP} \approx 1.582$ originating from the DP nature of the bottom-layer dynamics. Moreover, at the transition point, the avalanche clusters lose their compact shapes (see Fig. 8) and we should not expect the exponent relations (7)–(10), nor the calculation in Ref. [6] for the corrections to scaling to remain valid. In this section we will demonstrate the break down of mass hyperscaling relation (10) and how the avalanches affect the roughness of the sand surface.

A. Breakdown of mass hyperscaling

At the transition point, the bottom layer of an avalanche cluster follows the critical DP dynamics. Therefore, we should expect from the fractal DP cluster shape that the density of sites at the lowest $h = h_0$ level goes to zero in the thermodynamic limit for large avalanches. However, the overall shape of an avalanche consists, in addition, of sites at $h_0 + 1, h_0 + 2, \ldots$ levels. The higher-level sites that participate in the avalanche fill into the holes and voids next to the bottom layer cluster and more or less bring the avalanche cluster back to a compact shape. We can verify this compactness of the avalanche cluster by a direct measurement of the ratio $a/(lw)$, with a being the area of (or, the number of sites participating in) an avalanche. The result is shown as the solid line in Fig. 9. The approach to a finite value on the vertical axis demonstrates the compactness of the avalanche clusters by the existence of a finite area density ≈ 0.2 in the thermodynamic limit. The FSS estimates are plotted against $1/\ln y$ instead of $1/y$ since the roughness of the surface diverges only logarithmically in y, which will be elaborated later.

Contrary to a finite area density, as also shown in Fig. 9, the mass density $m/(lw\delta)$ (the dashed line) goes to zero in the thermodynamic limit. The absence of a finite mass density breaks the scaling

$$m \sim lwd, \tag{15}$$

which lead, in Ref. [5], to the mass hyperscaling relation (10). The plot of the combined exponent $\sigma - z - 2\alpha$ in Fig. 10 shows the violation of Eq. (10) as the FSS estimates approach ≈ 1.72 which is much lower than the expected value 2 for compact avalanches obeying Eq. (15).

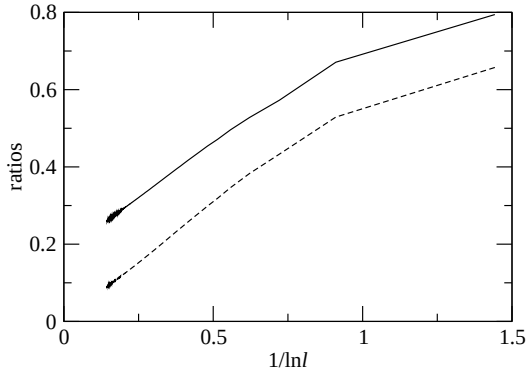

FIG. 9: The FSS plot of the area density $a/(lw)$ (solid line) and the mass density $m/(lw\delta)$ (dashed line) versus inverse the length logarithm $(1/\ln l)$ for the avalanche clusters at the DP transition point. While the area density converges to a finite value at the thermodynamic limit, the mass density converges to 0.

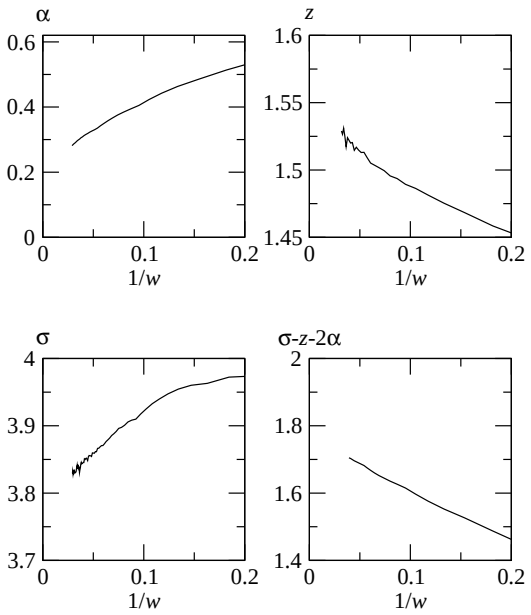

FIG. 10: FSS estimates of the scaling exponents derived from the avalanche exponents τ_l, τ_w, τ_δ for the discrete-height sandbox model versus the inverse width $(1/w)$ at the DP transition point. The z exponent is consistent with dynamic exponent of DP universality class $z_{\rm DP} \simeq 1.582$. The combination $\sigma - z - 2\alpha < 2$ indicates a violation of mass hyperscaling relation (10).

Also shown in Fig. 10 are the plots for the α, z, and σ exponents. They are consistent with $z = z_{\rm DP}$ and more or less with $\alpha = 0$. This confirms that the scaling behavior of the avalanches follows those of the SFRD interface. The slow convergence of α is to be expected from the logarithmic divergence of the interface roughness.

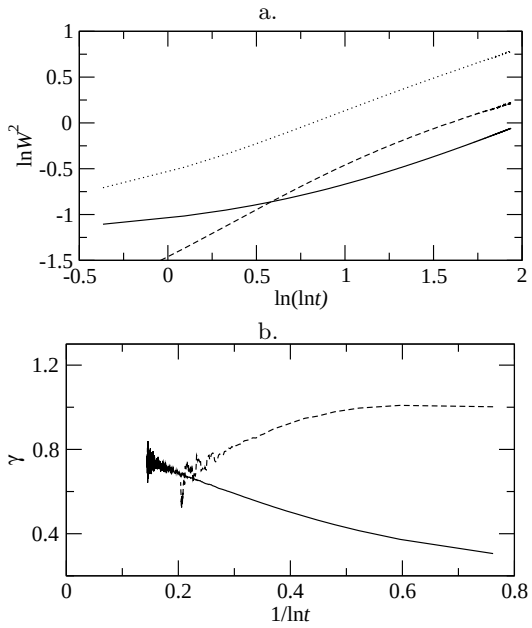

FIG. 11: (a) The roughness of a stationary DHSB surface(dotted line) compared with the roughness of the SFRD model (solid line) versus the double logarithm of time t at the DP transition point. The iterated avalanche process makes the surface rougher. The dashed line shows the difference $\Delta W^2 \equiv W^2_{\rm DHSB} - W^2_{\rm SFRD}$ between the roughness of the two. (b) FSS of the γ exponents of the logarithmic scaling for the SFRD roughness $W^2_{\rm SFRD}$ (solid line) and the difference ΔW^2 (dashed line), both assumed to have the scaling form $(\ln t)^\gamma$, versus the inverse of the logarithm of time. In the $t \to \infty$ limit, ΔW^2 scales with a smaller γ exponent than that of W^2.

B. Interface roughness

The remaining question is how the scaling behavior of the roughness is changed by the iterated avalanche process. We approach this by looking at the change of the global surface roughness itself and by comparing the scaling of this change to the scaling of the original interface roughness. The same analysis was performed in Ref. [6] which concerns only the $p = 1/2$ case of the DHSB, and it was found that the change in the global roughness by the avalanche process only represents large corrections to the KPZ scaling behavior of the surface. However, at the DP transition point, the interface roughness diverges only logarithmically. This makes the scaling of interface roughness more likely to be overwhelmed by the change in the roughness due to the avalanche process, and we generally would not expect the values of the scaling exponents to remain the same. In the following, we'll show the scaling of the interface does follow the same logarithmic divergence.

We perform a direct measurement of the global interface roughness at the transition point. The results are shown in Fig. 11(a). As in the $p = 1/2$ case, the surface is made rougher by the iterated avalanches. The increase

in the roughness ΔW^2 scale as $(\ln t)^{\gamma_\Delta}$ with the exponent $\gamma_\Delta \approx 0.4$ which is shown as the dashed line in Fig. 11(b). Since the interface roughness itself scales as $W^2 \sim (\ln t)^\gamma$ with $\gamma \approx 1$ which is shown as the solid line in Fig. 11(b), the change in the roughness is irrelevant comparing to the interface scaling. We can thus conclude that in the thermodynamics limit, the stationary surfaces of DHSB have the same γ exponent as the SFRD interfaces. Just as the in the deep phase ($p = 1/2$) of the the avalanche, the iterated avalanche process only gives rise to sizable corrections to the interface scaling behavior.

VIII. SUMMARY

In this article, we introduced the DHSB as a model for avalanches in granular materials with variable cohesiveness. This model exhibits a deepening transition from a shallow-avalanche phase where avalanches only involve a couple of surface layers of the granular material, into a deep-avalanche phase where the depths of avalanches increase as power laws in their lengths or widths. In the deep-avalanche phase, the scaling behavior of the avalanches belongs to the KPZ universality class: The avalanche clusters scale anisotropically with $l \sim w^{3/2}$ and depth increase as $\delta \sim w^{1/2}$. In the flat phase, the avalanche clusters scale isotropically $l \sim w$ with finite depths.

In both phases, the mass hyperscaling relation (10) based on compactness (15) of the avalanches holds. On the other hand, at the transition point, the hierarchical DP structure, pointed out by Täuber *et al.* [13], for each height level breaks this scaling in a subtle way. While the mass density $m/(lw\delta)$ of the avalanche clusters goes to zero in the thermodynamic limit, the area density $a/(lw)$ remains finite. However, the exact scaling behavior of the systems at this DP roughening transition point remains unclear even without the iterated avalanche in the DHSB model [14, 15, 16].

While we are not aware of any experimental study on how the avalanche behavior of a system will vary with a gradual change in the cohesiveness of the grains, the cohesiveness in granular system is known to vary with moisture [8] and grain sizes [4, 17]. We thus expect experimental studies in this direction to be feasible. The DHSB model represents a system with a layered structure where the heights are discrete, and the DP nature of the deepening transition relies heavily on a well-defined bottom layer or minimal stable configuration of the system. It thus wouldn't be a surprise if exact DP scaling were not to be observed in the avalanches of most experimental sandpiles. Nonetheless, the breakdown of the mass hyperscaling relation (10) comes from the fractal aspect of the hierarchical DP clusters and is a more fundamental property. It would serve as a hallmark of such a transition if it's to be observed experimentally.

The author thanks Marcel den Nijs for many helpful discussions and critical reading of the manuscript. This research is supported by the National Science Foundation under Grant No. DMR-9985806.

[1] P. Bak, C. Tang, and K. Wiesenfeld, Phys. Rev. Lett. **59**, 381 (1987).
[2] V. Frette *et al.*, Nature **379**, 49 (1996).
[3] K. Christensen *et al.*, Phys. Rev. Lett. **77**, 107 (1996).
[4] M. A. S. Quintanilla, J. M. Valverde, A. Castellanos, and R. E. Viturro, Phys. Rev. Lett. **87**, 194301 (2001).
[5] C.-C. Chen and M. den Nijs, Phys. Rev. E **65**, 031309 (2002).
[6] C.-C. Chen and M. den Nijs, Phys. Rev. E **66**, 011306 (2002).
[7] D. J. Hornbaker *et al.*, Nature **387**, 765 (1997).
[8] S. T. Nase, W. L. Vargas, A. A. Abatan, and J. J. McCarthy, Powder Technology **116**, 214 (2001).
[9] M. Kardar, G. Parisi, and Y.-C. Zhang, Phys. Rev. Lett. **56**, 889 (1986).
[10] J. Kertész and D. E. Wolf, Phys. Rev. Lett. **62**, 2571 (1989).
[11] U. Alon, M. R. Evans, H. Hinrichsen, and D. Mukamel, Phys. Rev. Lett. **76**, 2746 (1996).
[12] D. Dhar and R. Ramaswamy, Phys. Rev. Lett. **63**, 1659 (1989).
[13] U. C. Täuber, M. J. Howard, and H. Hinrichsen, Phys. Rev. Lett. **80**, 2165 (1998).
[14] U. Alon, M. R. Evans, H. Hinrichsen, and D. Mukamel, Phys. Rev. E **57**, 4997 (1998).
[15] J. M. López and H. J. Jensen, Phys. Rev. Lett. **81**, 1734 (1998).
[16] Y. Y. Goldschmidt, H. Hinrichsen, M. Howard, and U. C. Täuber, Phys. Rev. E **59**, 6381 (1999).
[17] J. M. Valverde, A. Castellanos, A. Ramos, and P. K. Watson, Phys. Rev. E **62**, 6851 (2000).